Origin of the orbital and spin ordering in rare-earth titanates

Julien Varignon,[1,*] Mathieu N. Grisolia,[1] Daniele Preziosi,[1] Philippe Ghosez,[2] and Manuel Bibes[1]
[1]*Unité Mixte de Physique, CNRS, Thales, Université Paris Sud, Université Paris-Saclay, 91767 Palaiseau, France*
[2]*Theoretical Materials Physics, Q-MAT, CESAM, Université de Liège (B5), B-4000 Liège, Belgium*

(Received 12 June 2017; revised manuscript received 9 November 2017; published 4 December 2017)

Rare-earth titanates $RTiO_3$ are Mott insulators displaying a rich physical behavior, featuring most notably orbital and spin orders in their ground state. The origin of their ferromagnetic to antiferromagnetic transition as a function of the size of the rare earth however remains debated. Here we show on the basis of symmetry analysis and *first-principles* calculations that although rare-earth titanates are nominally Jahn-Teller active, the Jahn-Teller distortion is negligible and irrelevant for the description of the ground state properties. At the same time, we demonstrate that the combination of two antipolar motions produces an effective Jahn-Teller-like motion which is the key of the varying spin-orbital orders appearing in titanates. Thus, titanates are prototypical examples illustrating how a subtle interplay between several lattice distortions commonly appearing in perovskites can produce orbital orderings and insulating phases irrespective of proper Jahn-Teller motions.

DOI: 10.1103/PhysRevB.96.235106

I. INTRODUCTION

ABO_3 oxide perovskites, with partly filled d states on the B site, exhibit a rich physical behavior originating from the intimate coupling between structural, electronic (charge and orbital), and magnetic degrees of freedom [1]. Typical examples are the rare-earth vanadates $R^{3+}V^{3+}O_3$ ($3d^2$-t_{2g}^2 electronic configuration on V^{3+} ions) that exhibit two different spin and orbital orders yielding distinct symmetries for the ground state at low temperature [2,3]. With the electronic degeneracy of Ti^{3+} $3d^1$-t_{2g}^1 configuration, rare-earth titanates $R^{3+}Ti^{3+}O_3$ are often expected to be another textbook example of such a subtle interplay between orbital and spin orders.

Rare-earth titanates are Mott insulators, which according to their small tolerance factor, adopt a common orthorhombic $Pbnm$ structure characterized by large oxygen cage rotations [4–6], i.e., $a^-a^-c^+$ antiferrodistortive motions in Glazer's notations [7]. They also all undergo a magnetic phase transition to either a ferromagnetic (FM) ordering for small R = Lu-Gd+Y or a G-type antiferromagnetic (G-AFM) ordering for large R = Sm-La [6,8,9].

The nature of the very peculiar FM to G-AFM transition as a function of the rare-earth size is however puzzling and controversial [9]. On one hand, Ti^{3+} is nominally a Jahn-Teller (JT) active ion and the JT distortion is commonly proposed as a key ingredient to explain the transition [10,11]. However, while such a distortion could be compatible with the ferromagnetic phase [12,13], it cannot provide a satisfying explanation for the purely antiferromagnetic phase [10]. On the other hand, some other works have proposed that the JT distortion is neither responsible for the insulating phase of these materials nor for the observed orbital orders [14,15].

Instead, Mochizuki *et al.* have suggested that specific orbital orderings for the FM and AFM phases are triggered by the crystal field produced by the rare earth [13,16], with a potential competition with the JT distortion [11]. This latter model ultimately results in combinations of the three t_{2g} orbitals [9,13,16,17] and now appears as a generic mechanism to yield the coupled spin-orbital orders in the ground state of $3d^1$ systems [14]. However, clear theoretical evidence of the individual role of each lattice distortion, including the ubiquitous oxygen cage rotations and/or rare-earths motions, is still missing.

In this article we revisit the nature of the orbital and spin orders in the ground state of rare-earth titanates on the basis of symmetry mode analysis and first-principles calculations. While the JT distortion appears rather negligible, we show that the combination of two specific antipolar distortions involving the rare earth produces an effective JT motion tuning the spin-orbital properties of the low temperature phase.

II. RESULTS

We first performed a symmetry-adapted mode analysis (with AMPLIMODES [18,19]) of some available experimental data in order to quantify the amplitude of distinct lattice distortions appearing in titanates. The results are summarized in Table I. As expected, all titanates develop strong antiferrodistortive motions—antiphase Φ_{xy}^- (R_5^- irreps) and in-phase Φ_z^+ (M_2^+ irreps) motions corresponding to $a^-a^-c^0$ and $a^0a^0c^+$ rotations, respectively [see Figs. 1(a) and 1(d)]—whose strengths are governed by steric effects. They also exhibit strong A_X (X_5^- irreps) and A_R (R_4^- irreps) distortions, involving antipolar motions of rare earth and/or coplanar oxygens in the (ab) plane as sketched in Figs. 1(b) and 1(c). These two modes also seem to be governed by steric effects, with a softening of their magnitude with increasing the rare-earth ionic radius albeit the R_4^- mode decreases more abruptly. Additionally, they also develop a Jahn-Teller (JT) distortion involving equatorial oxygen motions—two anions move inward, two outward—while apical oxygens are fixed [see Fig. 1(e)]. This motion being in phase between consecutive planes along the c axis, we label this JT mode as Q_2^+ (M_3^+ irreps) following Goodenough notation [21]. Surprisingly, this JT distortion is found very weak for all titanates, although it monotonously increases when going from Y to La. JT distortions are well known to be smaller for t_{2g} electrons than for e_g electrons but they remain here

*julien.varignon@cnrs-thales.fr

TABLE I. Amplitude of distortions (in Å) of some available experimental rare-earth titanates structures. The values for our optimized structures (0 K) are also reported. Experimental structures are taken from Ref. [11] at 8 K for $LaTiO_3$, and from Ref. [6] at 290, 100, 290, and 2 K for $NdTiO_3$, $SmTiO_3$, $GdTiO_3$, and $YTiO_3$, respectively. The Goldschmidt tolerance factor is given in parentheses and is extracted using a tolerance factor calculator from Ref. [20].

Mode	(t. factor)	Y [6] (0.831)	Gd [6] (0.890)	Sm [6] (0.898)	Nd [6] (0.908)	La [11] (0.927)
Φ^-_{xy} (R_5^-)	expt.	1.83	1.70	1.61	1.62	1.32
	calc.	1.95	–	–	–	1.44
Φ^+_z (M_2^+)	expt.	1.30	1.24	1.17	1.18	0.95
	calc.	1.34	–	–	–	1.04
A_X (X_5^-)	expt.	0.94	0.86	0.77	0.71	0.56
	calc.	0.99	–	–	–	0.66
Q_2^+ (M_3^+)	expt.	0.01	0.01	0.01	0.02	0.04
	calc.	0.02	–	–	–	0.05
A_R (R_4^-)	expt.	0.25	0.21	0.17	0.14	0.09
	calc.	0.29	–	–	–	0.11

one order of magnitude smaller than amplitudes appearing in the ground state of rare-earth vanadates (V^{3+} t^2_{2g} electronic degeneracy) [3]. This analysis of experimental structures therefore provides strong support to the relatively small contribution of the JT distortion in titanates suggested by former studies [15].

In order to gain microscopic insights on the relationship between these distortions and spin-orbital orders, we performed first-principles calculations using density functional

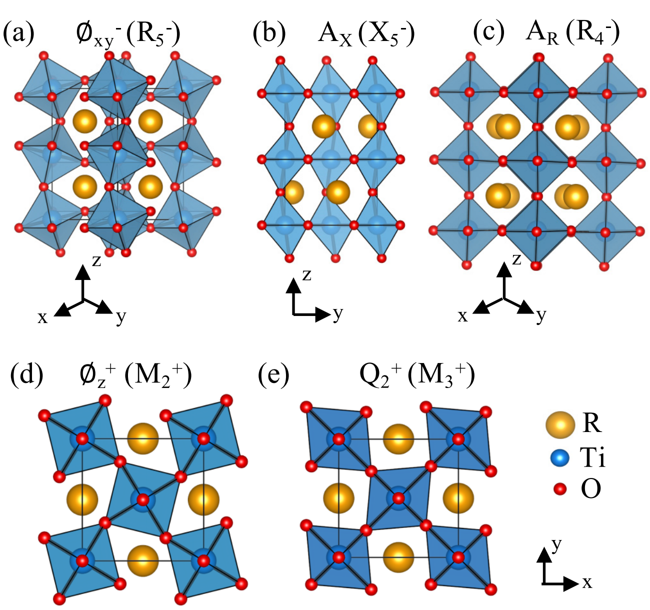

FIG. 1. Sketches of the lattice distortions appearing in rare-earth titanates ground state. (a) Antiphase Φ^-_{xy} (R_5^- irreps) oxygen cage rotation, (b) antipolar A_X (irreps X_5^-) motion, (c) antipolar A_R (R_4^- irreps) motion, (d) in phase Φ^+_z (M_2^+ irreps) oxygen cage rotation, and (e) Q_2^+ (M_3^+ irreps) Jahn-Teller motion. Note that amplitudes of distortions have been amplified on the sketches and are not representative of their magnitude in the ground state structure.

theory (DFT) with the Vienna *ab initio* simulation package [22,23]. We used the PBE functional revised for solids [24] in combination with effective Hubbard U_{eff} corrections [25] of 2.5 eV on Ti $3d$ levels and of 1 eV on the rare-earth $4f$ levels in order to account for the electronic correlations (see the Supplemental Material [26] for a detailed discussion on the choice of these parameters). We used the projector augmented waves (PAW) pseudopotentials [28] with the following valence electron configurations: $4s^2 3d^2$ (Ti), $2s^2 2p^4$ (O), $4s^2\ 4p^6 5s^2 5d^1 4f^0$ (Y), $5p^6 6s^2 5d^1 4f^0$ (La). An energy cutoff of 500 eV was used and we relaxed geometries until forces are lower than 1 meV/Å. A $6 \times 6 \times 4$ k-point grid was used to sample the Brillouin zone unless stated otherwise. We explored four different magnetic orderings during the calculations: ferromagnetic (FM), as well as A, C, and G-type antiferromagnetic solutions with spins treated only at the collinear level. We focus in this study on $YTiO_3$ and $LaTiO_3$ appearing as model systems to understand the Ti $3d$ electronic structure since they do not possess $4f$ electrons.

Geometry optimizations for these two compounds yield a $Pbnm$ ground state associated with a FM and a G-type AFM solution for $YTiO_3$ and $LaTiO_3$, respectively, consistently with experiments. While the stability of the FM solution of $YTiO_3$ is rather large ($\Delta E = -18.5$ meV/f.u. between the FM and G-AFM solutions), the stability of the G-AFM over the FM solution in $LaTiO_3$ is small ($\Delta E = -3.4$ meV/f.u.) likely underlying a weakly stable AFM solution. The extracted amplitude of distortions of our ground states are reported in Table I and are compatible with experimental reports, therefore validating our optimizations (lattice parameters and atomic positions are given in the Supplemental Material).

We then explored the origin of the orthorhombic structure by studying the energy potentials of the different lattice distortions. To that end, we have frozen some lattice motions in a hypothetical high-symmetry cubic structure ($Pm\bar{3}m$) having the volume of the ground state structure. Note that the k-point mesh is increased to $12 \times 12 \times 8$ in order to enhance both accuracy and convergence of the wave function. Figure 2 reports the energy landscapes for $YTiO_3$ (blue squares) and $LaTiO_3$ (red circles) using a FM configuration [29] (energy potentials using a G-type AFM configuration are reported in the Supplemental Material). As expected, the two oxygen cage rotations (Φ^-_{xy} and Φ^+_z modes) present double well potentials associated with strong energy gains and produce the orthorhombic $Pbnm$ symmetry. The antipolar A_X mode also develops a double well potential for $YTiO_3$ and $LaTiO_3$. The energy gain is larger for $YTiO_3$ albeit one order of magnitude smaller than that of the oxygen cage rotations. For both compounds, the antipolar A_R mode is always associated with a single well energy potential, indicating that this mode is not intrinsically unstable and the driving force of the ground state. Importantly, the JT distortion behaves differently for the two compounds: we do observe single well potentials for $YTiO_3$ and $LaTiO_3$ but the minimum is shifted to nonzero amplitude of the JT mode for $LaTiO_3$. It is worth noticing that we observe two distinct wells for $LaTiO_3$ depending on the sign of the lattice distortion. Therefore, it seems that in $LaTiO_3$, the JT distortion is able to produce an energy gain by favoring an orbital polarization. As inferred by the different behavior obtained for the two compounds, the ability of the JT distortion

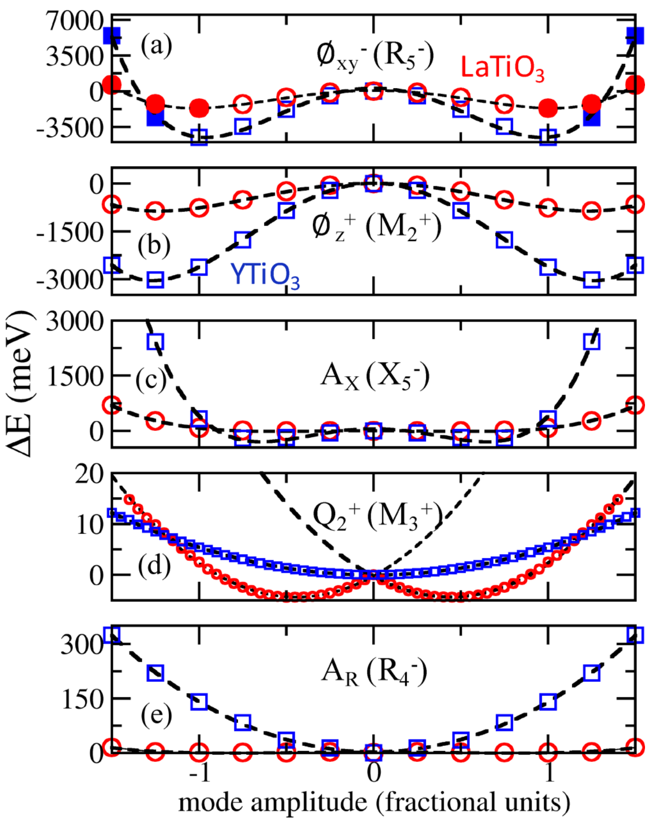

FIG. 2. Energy potentials with respect to the amplitude of distortion (in fractional units) of the different modes appearing in the ground state of $YTiO_3$ (blue squares) and $LaTiO_3$ (red circles), 1.00 representing the actual distortion appearing in the ground state of each material. Filled (unfilled) symbols represent insulating (metallic) solutions. Calculations have been performed in a pseudocubic unit cell having the volume of the ground state structure. (a) The Φ_{xy}^- mode ($a^-a^-c^0$ oxygen cage rotation). (b) The Φ_z^+ mode ($a^0a^0c^+$ oxygen cage rotation). (c) The A_X antipolar mode. (d) The Q_2^+ mode corresponding to a Jahn-Teller distortion. (e) The A_R antipolar mode. We emphasize that the k-point mesh is increased to $12 \times 12 \times 8$ in order to increase both accuracy and convergence of the energies.

to produce energy gains seems to highly rely on the tolerance factor or the unit cell volume. We can check this hypothesis in our calculations by computing the energy potentials of $YTiO_3$ and $LaTiO_3$ by using the volume of the other compound (results are presented in the Supplemental Material). When using $YTiO_3$ volume, the JT potential for $LaTiO_3$ becomes a single well potential whose energy minimum is located at zero amplitude of the JT mode. On the other hand, under a volume expansion, the minimum of the JT potential of $YTiO_3$ is shifted to a nonzero amplitude similar to the $LaTiO_3$ ground state [30]. This striking result is in close agreement with the experimental observation of a strengthening of the amplitude associated with the JT distortion with increasing the tolerance factor (see Table I). Finally, it is worth to emphasize that only large Φ_{xy}^- rotation either in the FM or G-AFM spin ordering for $YTiO_3$ and $LaTiO_3$—and large A_X antipolar modes in the G-AFM configuration for $YTiO_3$ (see the Supplemental Material)—are able to open a band gap.

III. DISCUSSION

Being not necessarily intrinsically unstable, the presence of the JT and antipolar A_R modes originates from the symmetry allowed terms in the free energy expansion $\mathcal{F}$ around a $Pm\bar{3}m$ cubic symmetry. Among all possible terms, $\mathcal{F}$ exhibits several trilinear couplings:

$$\begin{aligned}\mathcal{F} \propto\ & a\Phi_{xy}^-\Phi_z^+A_X + b\Phi_{xy}^-A_XQ_2^+\\ &+ c\Phi_z^+A_XA_R + dA_XA_RQ_2^+. \qquad (1)\end{aligned}$$

According to the first term, the condensation of the two rotations (Φ_{xy}^- and Φ_z^+ modes) automatically brings the antipolar A_X motion in the system in order to lower the energy, irrespective of its stability/instability. Subsequently, the second term of Eq. (1) will force the appearance of the JT distortion in any case. The latter therefore has an improper origin, a mechanism already discussed in some other systems [3,31,32] and that explains its small amplitude for titanates with low tolerance factor. Finally, according to the third term in Eq. (1), the A_R antipolar mode also appears as a consequence of the Φ_z^+ ($a^0a^0c^+$) oxygen cage rotation and the A_X antipolar motion.

These trilinear terms do not only explain the appearance of secondary Q_2^+, A_X, and A_R modes but are also the key to understand the different spin-orbital orders appearing in titanates. Although the two types of antipolar distortions [A_X (X_5^- irreps) and A_R (R_4^- irreps)] have a distinct symmetry, their product belongs to the irreducible representation of the JT motion ($X_5^-R_4^- = M_3^+$) as inferred by the fourth term of Eq. (1). Consequently, even in absence of significant pristine Q_2^+ distortion, their joint appearance corresponds to an effective Jahn-Teller motion that will drive orbital and spin orders. As the tolerance factor decreases from large to small R cations, the oxygen rotations (Φ_{xy}^- and Φ_z^+ modes) progressively increase, yielding larger antipolar motions (A_X and A_R modes) resulting from the first and third terms of Eq. (1) (see also Table I). Then, due to the effective JT character of these combined antipolar motions, their amplification produce an orbital ordering, comparable to the one that would be produced by a proper Q_2^+ mode and which is able to switch the magnetic ordering from G-type AFM to FM. Remarkably, as confirmed by Table I, the amplification of the effective JT mode is automatically accompanied by a reduction of the proper JT mode, indicating a competition between these two motions. The oxygen motions force together the appearance and direction of the Q_2^+, A_X, and A_R modes through the first three terms in Eq. (1). Then, the fourth term teaches us if the joint presence of these modes is by itself energetically favorable, the d coefficient of Eq. (1) is always found positive meaning that the $A_XA_RQ_2^+$ trilinear term corresponds to an energy penalty whose contribution has to be minimized. This progressive disappearance of the Q_2^+ distortion as the tolerance factor decreases further confirms its negligible character, and *de facto* the importance of the effective JT motions, on the spin-orbital properties of rare-earth titanates.

We can check the role of the effective Jahn-Teller motion in our calculations by analyzing in details the electronic and magnetic properties of $YTiO_3$ and $LaTiO_3$. We observe that both $YTiO_3$ and $LaTiO_3$ are insulators in our simulations with band gaps of 1.04 and 0.94 eV, respectively, compatible with experimental reports on different titanates [33–37]. Our

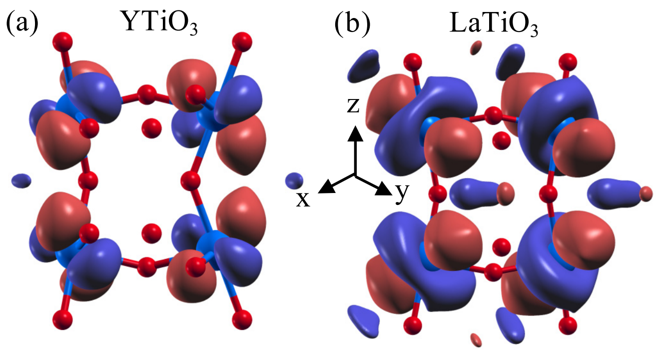

FIG. 3. Orbital orderings developed by our optimized ground state of $YTiO_3$ (a) and $LaTiO_3$ (b).

computed magnetic moments on Ti^{3+} are evaluated around 0.94 and 0.84 μ_B for $YTiO_3$ and $LaTiO_3$, respectively, and agree with experiments although the latter value is slightly overestimated [5,38]. However, all Ti sites are occupied by only one electron.

In the search of the localization of this single Ti-d electron, we built the maxi-localized Wannier functions (MLWFs) for the ground state of both materials using the Wannier90 software [39–41]. First, we have followed the strategy discussed in Ref. [42]. We have initially projected the Kohn-Sham states onto three generic t_{2g} orbitals per Ti sites in order to extract the initial gauge matrix for the localization procedure. The latter is then restricted to the occupied manifold in order to extract only occupied levels, albeit it is reduced to bands with dominant O and Ti characters. The optimization renders only one t_{2g}-like MLWFs per Ti site, and other MLWFs results in O-p states in the vicinity of Ti sites. It further confirms the occupancy of Ti 3d states by a single electron, whose localization renders the orbital orderings depicted in Fig. 3. These orbital orderings are very similar to those reported on the basis of dynamical mean field theory calculations [14] as well as Ref. [43] for $YTiO_3$ and Refs. [11,16] for $LaTiO_3$. However, the shape of the resulting t_{2g} orbital on each Ti site cannot be explained by a single electron lying in a particular t_{2g} orbital [13]. We can deduce the different contributions of the t_{2g} levels on the orbital ordering by using different set of bands for the localization procedure. To that end, we considered a total of 12 bands corresponding to dominantly Ti t_{2g} contributions located around the Fermi level E_F, i.e., four bands below E_F, eight bands above E_F. We then integrate the density of states projected on the new t_{2g}-like WFs up to the Fermi level in order to extract their contribution to the orbital ordering [44]. We end with very different contributions of the t_{2g} states to the resulting orbital ordering:

$$|\Psi_{\mathrm{YTiO_3}}\rangle \propto 0.686|d_{xy}\rangle + 0.728(\alpha|d_{xz}\rangle + \beta|d_{yz}\rangle), \quad (2)$$

$$|\Psi_{\mathrm{LaTiO_3}}\rangle \propto 0.565|d_{xy}\rangle + 0.825(\alpha|d_{xz}\rangle + \beta|d_{yz}\rangle), \quad (3)$$

where α and β are coefficients describing the contribution of both d_{xz} and d_{yz} locally on each Ti site ($\alpha^2 + \beta^2 = 1$). It then appears that going from R =Y to R = La, the orbital ordering changes from a rather well balanced combination of the d_{xy} and $(d_{xz} + d_{yz})$ orbitals to a dominant $(d_{xz} + d_{yz})$ character [13,14].

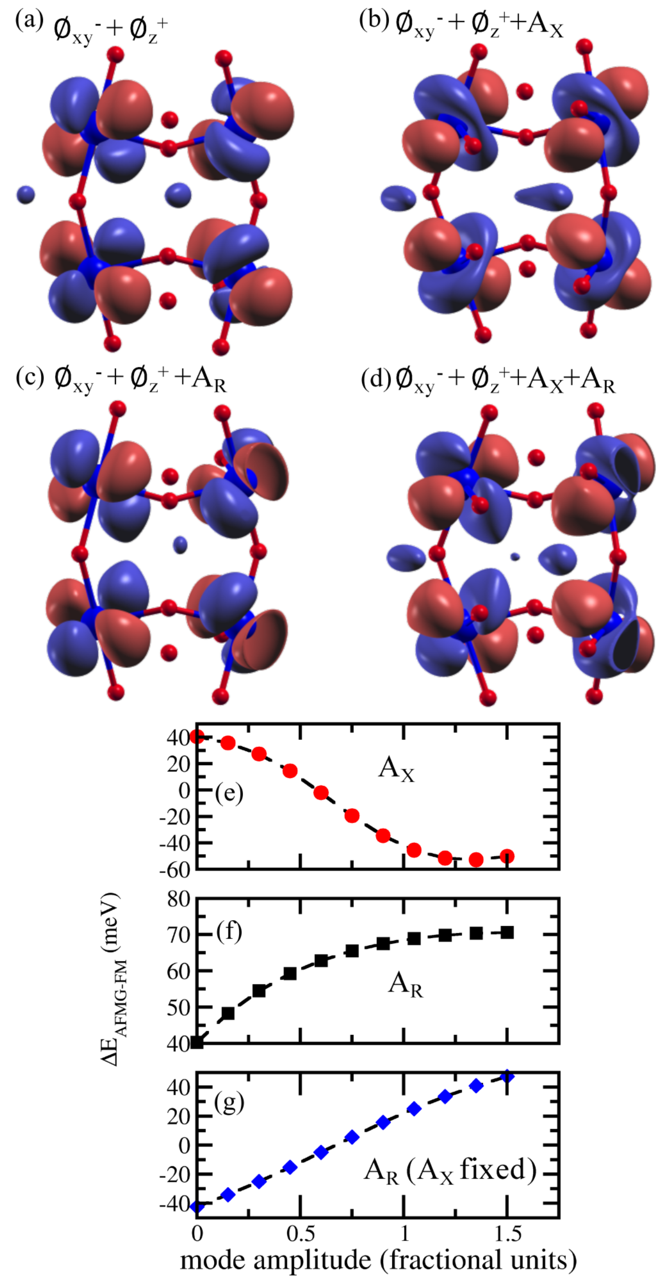

FIG. 4. Influence of the rare-earth motions on the orbital and spin degrees of freedom. (a) Orbital ordering appearing with only the two oxygen cage rotations. (b) Orbital ordering obtained by freezing the antipolar A_X motion with the two rotations. (c) Orbital ordering obtained by freezing the antipolar A_R motion with the two rotations. (d) Orbital ordering obtained by freezing the antipolar A_R motion with the two rotations and the antipolar A_X mode. (e) and (f) Energy difference between the G-AFM and FM solutions when adding either the antipolar A_X (e), A_R (f) antipolar motions to the system with the rotations. (g) Energy difference between the G-AFM and FM solutions when adding the antipolar A_R mode to the system with rotations and the A_X mode.

To gain insights on whether the contributions of the antipolar distortions and the existence of the effective JT mode drive the varying spin-orbital orders in titanates, we can track the evolution of the orbital ordering upon condensing different lattice modes appearing in $YTiO_3$ in an ideal cubic phase having the ground state volume. Starting from a structure with the two oxygen cage rotations, we obtain an orbital ordering resembling that of $YTiO_3$ [see Fig. 4(a)] with a minimal d_{xy} orbital contribution ($|\Psi\rangle \propto 0.360|d_{xy}\rangle + 0.933(\alpha|d_{xz}\rangle + \beta|d_{yz}\rangle)$). On the one hand, adding the A_X antipolar mode to the two rotations strongly suppresses the d_{xy} character of the orbital ordering, the latter almost vanishes ($|\Psi\rangle \propto 0.224|d_{xy}\rangle + 0.975(\alpha|d_{xz}\rangle + \beta|d_{yz}\rangle)$, and therefore the orbital order is very similar to that of $LaTiO_3$ [see Fig. 4(b)]. On the other hand, adding the A_R antipolar motion to the rotations completely switches the weight of the d_{xy} and d_{xz}/d_{yz} character ($|\Psi\rangle \propto 0.706|d_{xy}\rangle + 0.709(\alpha|d_{xz}\rangle + \beta|d_{yz}\rangle)$) with an orbital ordering now resembling that of $YTiO_3$ [see Fig. 4(c)]. Looking at the energy difference between FM and G-AFM solutions when condensing independently the two antipolar motions to the rotations, we observe that the A_R mode favors a FM ordering while the A_X mode strongly enhances the stability of G-AFM solution [see Figs. 4(e) and 4(f)].

Therefore, starting from a structure with oxygen cage rotations and the sole A_X antipolar mode, all titanates should exhibit an antiferromagnetic ordering of the Ti^{3+} lattice [see Fig. 4(g)]. However, upon adding the A_R lattice distortion, the effective JT mode enters and is able to enhance the d_{xy} character of the orbital ordering ($|\Psi\rangle \propto 0.419|d_{xy}\rangle + 0.908(\alpha|d_{xz}\rangle + \beta|d_{yz}\rangle)$) and to stabilize the FM ordering over the G-AFM solution [see Figs. 4(d) and 4(g)]. We emphasize that the stability of the FM order versus the G-AFM order is strongly enhanced in comparison to the case of the sole condensation of A_R with the rotations, further proving the importance of the effective JT mode on the varying spin-orbital properties of titanates. Finally, we observe that the tetragonality $c/\sqrt{2}a$ of the unit, scaling with the oxygen cage rotations amplitude, further increases the d_{xy} contribution to the orbital-order stabilizing the FM solution. It is worth to emphasize that we do observe that the Q_2^+ mode has a rather marginal effect leaving the weight of the three t_{2g} orbitals on the orbital ordering unchanged.

IV. CONCLUSION

In conclusion, our first-principles simulations highlight the subtle interplay between structural, orbital, and spin degrees of freedom in rare-earth titanates. Most notably, we have shown that, in spite of the absence of sizable proper JT distortions, the oxygen rotations inherent to the *Pbnm* phase drive the appearance of two distinct antipolar rare-earth motions, which together correspond to an effective JT distortion. As the tolerance factor decreases, these antipolar motions increases together with the oxygen rotations and promote an orbital ordering similar to that which would be produced by proper JT motions and favors a FM spin order explaining the change of ground state from La to Y. The antipolar motions being generic to any perovskite adopting a *Pbnm* structure, this study demonstrates that it is possible to achieve orbital orders and insulating phases in these materials irrespectively of proper Jahn-Teller distortions.

ACKNOWLEDGMENTS

This work has been supported by the European Research Consolidator (ERC) grant MINT under the Contract No. 615759. Calculations took advantages of the Occigen machines through the DARI project EPOC A0020910084 and of the DECI resource FIONN in Ireland at ICHEC through the PRACE project FiPSCO. Ph.G. acknowledges support from the ARC project AIMED and F.R.S-FNRS PDR Project No. HiT4FiT. J.V. is very grateful to J. Íñiguez for his initiation to Wannier functions. Authors acknowledge J. Santamaria for fruitful discussions.

[1] P. Zubko, S. Gariglio, M. Gabay, P. Ghosez, and J.-M. Triscone, Annu. Rev. Condens. Matter Phys. **2**, 141 (2011).
[2] S. Miyasaka, Y. Okimoto, M. Iwama, and Y. Tokura, Phys. Rev. B **68**, 100406 (2003).
[3] J. Varignon, N. C. Bristowe, E. Bousquet, and P. Ghosez, Sci. Rep. **5**, 15364 (2015).
[4] J. Greedan, J. Less-Common Met. **111**, 335 (1985).
[5] M. Eitel and J. Greedan, J. Less-Common Met. **116**, 95 (1986).
[6] A. C. Komarek, H. Roth, M. Cwik, W.-D. Stein, J. Baier, M. Kriener, F. Bourée, T. Lorenz, and M. Braden, Phys. Rev. B **75**, 224402 (2007).
[7] A. M. Glazer, Acta Crystallogr. Sect. B **28**, 3384 (1972).
[8] T. Katsufuji, Y. Taguchi, and Y. Tokura, Phys. Rev. B **56**, 10145 (1997).
[9] M. Mochizuki and M. Imada, New J. Phys. **6**, 154 (2004).
[10] T. Mizokawa, D. I. Khomskii, and G. A. Sawatzky, Phys. Rev. B **60**, 7309 (1999).
[11] M. Cwik, T. Lorenz, J. Baier, R. Müller, G. André, F. Bourée, F. Lichtenberg, A. Freimuth, R. Schmitz, E. Müller-Hartmann, and M. Braden, Phys. Rev. B **68**, 060401 (2003).
[12] M. Mochizuki and M. Imada, J. Phys. Soc. Jpn. **69**, 1982 (2000).
[13] M. Mochizuki and M. Imada, J. Phys. Soc. Jpn. **70**, 2872 (2001).
[14] E. Pavarini, S. Biermann, A. Poteryaev, A. I. Lichtenstein, A. Georges, and O. K. Andersen, Phys. Rev. Lett. **92**, 176403 (2004).
[15] E. Pavarini, A. Yamasaki, J. Nuss, and O. K. Andersen, New J. Phys. **7**, 188 (2005).
[16] M. Mochizuki and M. Imada, Phys. Rev. Lett. **91**, 167203 (2003).
[17] J. Akimitsu, H. Ichikawa, N. Eguchi, T. Miyano, M. Nishi, and K. Kakurai, J. Phys. Soc. Jpn. **70**, 3475 (2001).
[18] D. Orobengoa, C. Capillas, M. I. Aroyo, and J. M. Perez-Mato, J. Appl. Crystallogr. **42**, 820 (2009).
[19] J. Perez-Mato, D. Orobengoa, and M. Aroyo, Acta Crystallogr. Sect. A **66**, 558 (2010).
[20] See http://www.me.utexas.edu/~benedekgroup/ ToleranceFactorCalculator for the tolerance factor calculator provided by Nicole Benedek.
[21] J. B. Goodenough, Annu. Rev. Mater. Sci. **28**, 1 (1998).
[22] G. Kresse and J. Hafner, Phys. Rev. B **47**, 558(R) (1993).
[23] G. Kresse and J. Furthmüller, Comput. Mater. Sci. **6**, 15 (1996).

[24] J. P. Perdew, A. Ruzsinszky, G. I. Csonka, O. A. Vydrov, G. E. Scuseria, L. A. Constantin, X. Zhou, and K. Burke, Phys. Rev. Lett. **100**, 136406 (2008).

[25] S. L. Dudarev, G. A. Botton, S. Y. Savrasov, C. J. Humphreys, and A. P. Sutton, Phys. Rev. B **57**, 1505 (1998).

[26] See Supplemental Material at http://link.aps.org/supplemental/10.1103/PhysRevB.96.235106 for which includes Refs. [6,11,25,27]. Rare-earth titanates are Mott insulators featuring in their ground state a striking ferromagnetic to antiferromagnetic phase transition as a function of the rare-earth radius. Using symmetry mode analysis, first-principles simulations and a Wannier analysis, we show that although titanates are nominally Jahn-Teller active with their $3d^1$ electronic configuration, the Jahn-Teller distortion is irrelevant for the description of the ground state properties. Alternatively, we demonstrate that a combination of antipolar motions produces a Jahn-Teller-like motion which is the key of the varying spin-orbital properties of these materials.

[27] A. I. Liechtenstein, V. I. Anisimov, and J. Zaanen, Phys. Rev. B **52**, R5467 (1995).

[28] P. E. Blöchl, Phys. Rev. B **50**, 17953 (1994).

[29] We note that it is nearly impossible to converge the electronic wave function for single lattice distortions using the G-AFM order.

[30] We note here that when using the $LaTiO_3$ ground state volume, the Jahn-Teller Q_2^+ motion develops an electronic instability for both $YTiO_3$ and $LaTiO_3$. Indeed at zero amplitude of the Q_2^+ mode, an energy gain of 1.90 and 0.57 meV is achieved for $YTiO_3$ and $LaTiO_3$, respectively, when the symmetry of the wave function is removed in the calculation, meaning that the electronic wave function does naturally want to distort to get rid of the electronic degeneracy.

[31] J. Varignon, N. C. Bristowe, and P. Ghosez, Phys. Rev. Lett. **116**, 057602 (2016).

[32] N. C. Bristowe, J. Varignon, D. Fontaine, E. Bousquet, and P. Ghosez, Nat. Commun. **6**, 6677 (2015).

[33] T. Arima, Y. Tokura, and J. B. Torrance, Phys. Rev. B **48**, 17006 (1993).

[34] Y. Okimoto, T. Katsufuji, Y. Okada, T. Arima, and Y. Tokura, Phys. Rev. B **51**, 9581 (1995).

[35] I. Loa, X. Wang, K. Syassen, H. Roth, T. Lorenz, M. Hanfland, and Y.-L. Mathis, J. Phys.: Condens. Matter **19**, 406223 (2007).

[36] M. N. Grisolia, F. Y. Bruno, D. Sando, H. J. Zhao, E. Jacquet, X. M. Chen, L. Bellaiche, A. Barthélémy, and M. Bibes, Appl. Phys. Lett. **105**, 172402 (2014).

[37] L. Bjaalie, A. Verma, B. Himmetoglu, A. Janotti, S. Raghavan, V. Protasenko, E. H. Steenbergen, D. Jena, S. Stemmer, and C. G. Van de Walle, Phys. Rev. B **92**, 085111 (2015).

[38] J. Goral and J. Greedan, J. Magn. Magn. Mater. **37**, 315 (1983).

[39] A. A. Mostofi, J. R. Yates, Y.-S. Lee, I. Souza, D. Vanderbiltd, and N. Marzari, Comput. Phys. Commun. **178**, 685 (2008).

[40] N. Marzari and D. Vanderbilt, Phys. Rev. B **56**, 12847 (1997).

[41] I. Souza, N. Marzari, and D. Vanderbilt, Phys. Rev. B **65**, 035109 (2001).

[42] J. Varignon, M. N. Grisolia, J. Íñiguez, A. Barthélémy, and M. Bibes, npj Quantum Mater. **2**, 21 (2017).

[43] H. Sawada and K. Terakura, Phys. Rev. B **58**, 6831 (1998).

[44] The Cartesian axes have been aligned along Ti-O directions in order to extract as much as possible pure t_{2g} orbitals.